OPEN

NPG Asia Materials (2017) 9, e366; doi:10.1038/am.2017.42
www.nature.com/am

ORIGINAL ARTICLE

Peptide-mediated core/satellite/shell multifunctional nanovehicles for precise imaging of cathepsin B activity and dual-enzyme controlled drug release

Fenfen Zheng, Penghui Zhang, Yu Xi, Kaikai Huang, Qianhao Min and Jun-Jie Zhu

Intracellular imaging of pathologically relevant proteases can provide essential information for the accurate evaluation of disease stage and progression. However, the risks of degradation by nonspecific enzymes during transportation and poor cellular uptake limit the use of peptide-based molecular probes (PMPs) for *in situ* protease imaging. To overcome these obstacles, a self-protected nanovehicle with a peptide-mediated core/satellite/shell structure was constructed for precise imaging of the protease cathepsin B (Cat B) *in situ* and the subsequent Cat B-responsive drug release. The self-protected nanovehicles demonstrated excellent resistance to nonspecific enzymolysis, thereby keeping the embedded PMPs intact until they reach the target organelle. Furthermore, the targeting ability of the outer shell facilitated the internalization of nanovehicles into tumor cells via receptor-guided recognition: the protective shell thereafter degraded in the intracellular microenvironment, and Cat B activity was dynamically monitored as the core/satellite structure disassembled. Meanwhile, the peptide-mediated satellite/shell structures served as three-dimensional gatekeepers to lock doxorubicin inside the nanovehicles, and drug release was spatiotemporally controlled by Cat B activity. This study provides important guiding principles for the rational design of self-protected nanovehicles for accurate diagnosis and therapy.
NPG Asia Materials (2017) **9,** e366; doi:10.1038/am.2017.42; published online 31 March 2017

INTRODUCTION

More than 600 proteases are encoded in the human genome, such as aspartic, cysteine, metallo-, serine and threonine proteases, and they perform essential functions in a variety of biological processes.[1] The abnormal expression of certain proteases is closely related to numerous human pathologies, including arthritis,[2] neurodegenerative disorders,[3] inflammatory processes,[4] cardiovascular diseases[5] and cancers.[6] Therefore, the development of chemical tools for *in situ* imaging of protease activity has gained considerable interest in recent years. A series of peptide-based molecular probes (PMPs) containing a signal donor and acceptor pair have been developed,[7–10] which translate enzymatic cleavage into detectable signals and provide promising noninvasive means to study cellular activities at the molecular level.

However, once exposed to the physiological environment, PMPs have poor stability and are easily degraded by nonspecific enzymes. Undesirable false signals resulting from nonspecific degradation represent a major limitation for the precise detection of protease activity. In addition, the lack of targeting ability may lead to poor cellular uptake, which also impedes imaging of the activity of the target protease. To overcome these obstacles, there is an urgent need to develop a nanoprobe that is capable of specifically accumulating in target cells, translating protease activity into physical signals and resisting premature degradation during transportation. It remains a significant challenge to develop structurally stable, selective and cell-permeable PMPs for assaying the function of a distinct protease in the complex milieu of the cell. If the resulting PMPs are protected by a stimulus-responsive shell with targeting ability, nonspecific cleavage of the peptide substrates by bulk proteases may be avoided, and cellular uptake would be facilitated by target–receptor interactions when the probes are applied in cellular or whole-animal imaging experiments.

In recent years, the stimulus-responsive dissociation strategy has been widely adopted in the design of nanocarriers for controlled drug release, shielding drugs during transportation but exposing when they reach the targeted domain.[11–14] These synthetic systems utilize an assortment of endogenous stimuli (pH,[15] ATP,[16] enzyme[17] or redox gradients[18]) or exogenous stimuli (changed temperature,[19] magnetic field,[20] ultrasound,[21] light[22] or electric pulses[23]) to facilitate targeted drug delivery in a spatial-, temporal- and dosage-controlled fashion. Inspired by these studies, we are considering the possibility that this strategy would be able to protect PMPs from nonspecific degradation and improve their cell uptake by virtue of receptor-guided recognition. In addition, protease cleavage is an important step in the release of

State Key Laboratory of Analytical Chemistry and Collaborative Innovation Center of Chemistry for Life Sciences, School of Chemistry & Chemical Engineering, Nanjing University, Nanjing, People's Republic of China
Correspondence: Associate Professor Q Min or Professor J-J Zhu, State Key Laboratory of Analytical Chemistry and Collaborative Innovation Center of Chemistry for Life Sciences, School of Chemistry & Chemical Engineering, Nanjing University, 22 Hankou Road, Nanjing 210093, People's Republic of China.
E-mail: minqianhao@nju.edu.cn or jjzhu@nju.edu.cn
Received 30 October 2016; revised 19 December 2016; accepted 21 January 2017

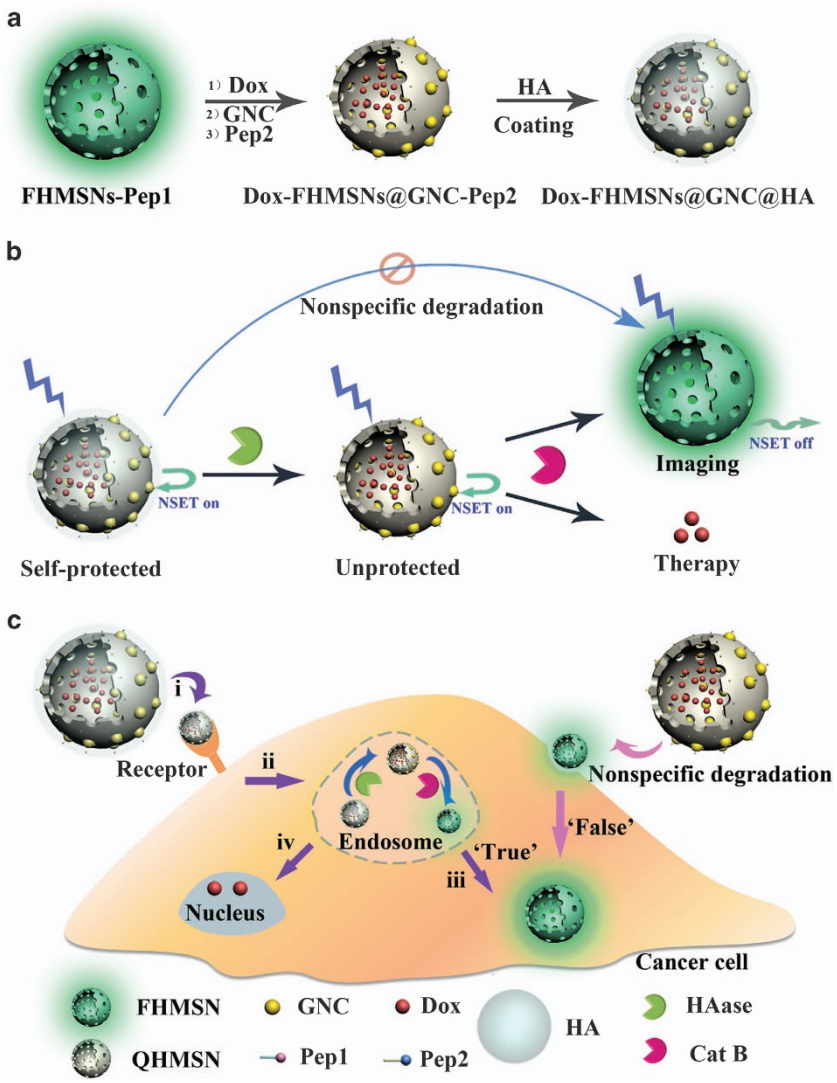

Scheme 1 Schematic illustration of the self-protected nanovehicles for *in situ* imaging of Cat B and dual-enzyme controlled drug release. (**a**) The preparation of the self-protected nanovehicles. (**b**) The disassembly of the self-nanovehicles based on enzyme cascade reactions with HAase and Cat B as triggers. (**c**) Targeted delivery, controlled release and intracellular imaging: (i) specific uptake via receptor-mediated endocytosis; (ii) accumulation in endosomes; (iii) endosomal escape and intracellular Cat B imaging; (iv) dual-enzyme triggered Dox release. Cat B, cathepsin B; HAase, hyaluronidase.

anticancer drugs from the enzymatically responsive nanocarriers, with the release rate being a function of active enzyme concentration.[24] Therefore, the capacity to precisely detect protease activity would aid in regulating of drug release behavior.

Herein, multifunctional stimulus-responsive nanovehicles were constructed *via* peptide-mediated core/satellite/shell assembly for targeted protease imaging and controlled drug release (Scheme 1). In this system, gold nanoclusters (GNCs, fluorescence acceptors) were assembled onto fluorescent, hollow mesoporous silica nanoparticles (FHMSNs, fluorescence donors) through the conjugation of peptide 1 (Pep1, a substrate of cathepsin B (Cat B)) to form PMPs (FHMSNs@GNC) with a core/satellite structure. The system can be specifically disassembled by Cat B, a lysosomal cysteine protease overexpressed in a wide variety of human cancers.[6,25] The GNCs were shown to quench the fluorescence of FHMSNs by nanometal surface energy transfer (NSET). Then, hyaluronic acid (HA) molecules were assembled on the surface *via* peptide 2 (Pep2), which specifically binds to HA with a dissociation constant of 10^{-7},[26] and HA then served as a shell that protected against nonspecific enzyme cleavage and an efficient target ligand for recognizing the CD44 and RHAMM receptors, which are overexpressed on the surface of cancer cells.[27,28] The above peptide-mediated core/satellite/shell nanocomplexes can be utilized as multifunctional nanovehicles for precise and dynamic imaging of Cat B and of controlled drug release, with the HA shell providing specific recognition and a protecting shell, the FHMSNs being drug carriers and signal generators, the GNC complexes being gatekeepers and signal inhibitors, and Cat B and hyaluronidase (HAase)[29] being dual openers and signal triggers. This self-protected peptide-based nanovehicle offers new avenues for the development of theranostic nanomedicine systems that could used for diagnosis, for therapy and for monitoring the delivery of drug molecules.

MATERIALS AND METHODS

Materials

All chemicals are listed in Supplementary Information and were used as received. All aqueous solutions were prepared using ultrapure water from a Milli-Q system (Millipore, USA). The peptides were purchased from GL Biochem Ltd. (Shanghai,

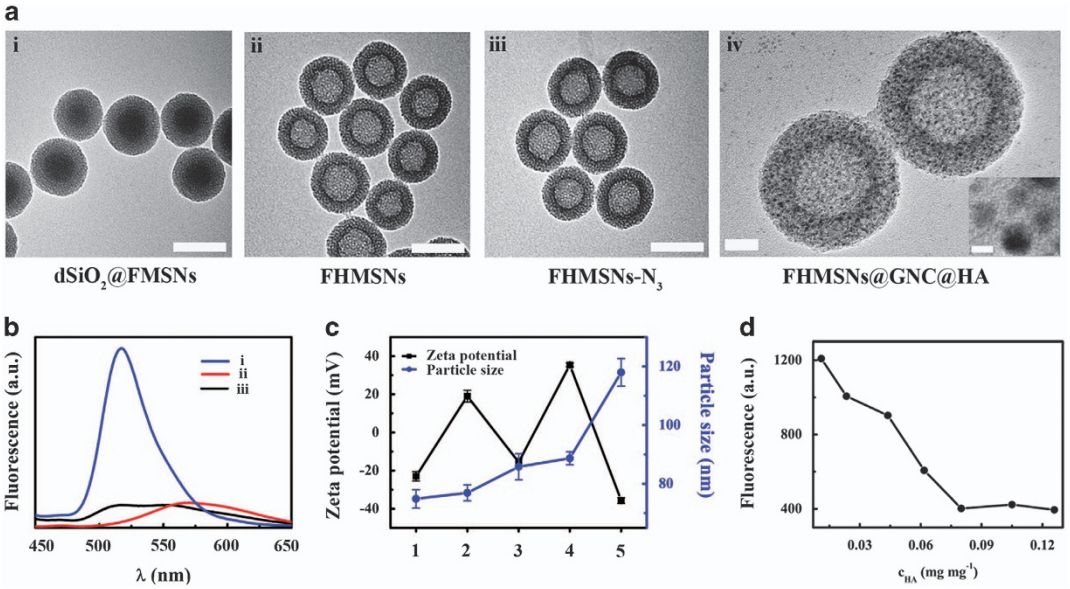

Figure 1 (**a**) TEM images of $dSiO_2$@FMSNs (i), FHMSNs (ii), and FHMSNs-N_3 (iii) (The scale bar is 100 nm), HRTEM images of FHMSNs@GNC@HA (iv) (The scale bar is 20 nm, the inset is a locally magnified version of figure d, and the scale bar is 2 nm). (**b**) Fluorescence emission spectra of (i) FHMSNs-Pep1, (ii) GNCs and (iii) FHMSNs@GNC. (**c**) The variations in zeta potential values and hydrodynamic size distributions during the assembly of the nanovehicles (1: FHMSNs, 2: FHMSNs-Pep1, 3: FHMSNs@GNC, 4: FHMSNs@GNC-Pep2, 5: FHMSNs@GNC@HA). (**d**) The fluorescent spectra of the nanovehicles with different HA densities treated with a nonspecific enzyme mixture. FHMSNs, fluorescent, hollow mesoporous silica nanoparticles; GNCs, gold nanoclusters; HA, hyaluronic acid; HRTEM, high-resolution transmission electron microscopy; Pep1, peptide 1.

China). The peptide sequences for preparing nanovehicles were as follows: P1: CRRGGKKGGKKRK (Pra); P2: CRRDDGAHWQFNALTVR.

Preparation of self-protected nanovehicles for Cat B detection

First, 200 µl FHMSNs-Pep1 (5 mg ml^{-1}) was mixed with 200 µl GNCs (5 mg ml^{-1}) and shaken for 6 h at 37 °C at a speed of 200 r.p.m. to form FHMSNs@GNC. The nanoparticles were centrifuged and washed thoroughly with PBS (10 mM, pH 7.4) to remove unreacted GNCs. The fluorescence spectrum of the supernatant at 560 nm was measured to calculate the loading amounts of GNCs on the FHMSNs-Pep1. The obtained results showed that the loading amount of GCs was 314 µg mg^{-1}. Then, 200 µl Pep2 was added to the FHMSNs@GNC solution, and the solution was incubated for 6 h at 37 °C at a speed of 200 r.p.m. to form FHMSNs@GNC-Pep2. Finally, HA was added, and the mixture was gently stirred for 1 h to form FHMSNs@GNC@HA. The resulting nanoparticles were centrifuged and washed thoroughly with PBS (10 mM, pH 7.4) to remove unreacted HA. The loading efficiency of HA on the FHMSNs@GNC was quantified using the published hexadecyltrimethylammonium bromide turbidimetric method.[28] The concentrations of protease enzyme Cat B in solution were detected by monitoring the fluorescence increase due to the cleavage of the Pep1 substrate by FHMSNs@GNC (unprotected nanovehicles) or FHMSNs@GNC@HA (self-protected nanovehicles).

Cat B detection *in vitro*

Briefly, 100 µl of the self-protected nanovehicles or unprotected nanovehicles (10 mg ml^{-1}) was incubated with 1) a nonspecific enzyme mixture (a mixture of trypsin (2 µg ml^{-1}), chymotrypsin (2 µg ml^{-1}) and MMP-2 (2 µg ml^{-1})) for 1 h at 37 °C; 2) CB (8 U ml^{-1}) for 1 h at 37 °C; 3) HAase (0.5 mg ml^{-1}) for 2 h at 37 °C; 4) HAase (0.5 mg ml^{-1}) for 2 h at 37 °C and then Cat B (8 U ml^{-1}) for another 1 h at 37 °C; 5) HAase (0.5 mg ml^{-1}) for 2 h at 37 °C and then different concentrations of Cat B for another 1 h at 37 °C. The fluorescence was detected at the excitation wavelength of 488 nm using a fluorescence spectrophotometer.

Intracellular Cat B imaging and dual-enzyme controlled drug release

In the logarithmic growth phase, the cells were incubated with different nanovehicles in cultured medium for different times. The amounts of the nanovehicles internalized into the cells were evaluated by confocal laser scanning microscopy (CLSM) and flow cytometry. For the detection of intracellular Cat B, the cells were treated with the nanovehicles for 6 h and then washed with PBS and cultured with fresh medium. The fluorescence signals were recorded by flow cytometry or CLSM. In the controlled drug release experiment triggered by intracellular HAase and Cat B, the cells were treated with the nanovehicles for different durations and monitored by CLSM. Cell viability was measured by an MTT assay.

RESULTS AND DISCUSSION

Fabrication and characterization of self-protected nanovehicles

The FHMSNs were synthesized by doping fluorescein isothiocyanate into the HMSNs according to the reported protocol with some modifications.[30] The obtained FHMSNs had a uniform size of 80 nm with a 20-nm-thick shell and displayed strong fluorescence, remarkable photostability and good biocompatibility, thus facilitating the *in situ* detection of Cat B and the tracking of intracellular drug delivery (Supplementary Figures S1a,b and S2). A specific surface area of 291.428 $m^2 g^{-1}$ and an average mesopore diameter of 3 nm for the as-synthesized FHMSNs were observed by Brunauer–Emmett–Teller (BET) analysis and Barret–Joyner–Halenda (BJH) analysis, respectively (Supplementary Figure S3). Small-angle X-ray diffraction analysis showed that the FHMSNs possessed well-ordered porous structures with wormlike arrangements (Supplementary Figure S4). These FHMSNs were then functionalized with 3-azidopropyltrimethoxysilane (FHMSNs-N_3) and tethered with propargyl-modified peptide 1 (Pep1) via copper (I)-catalyzed azide-alkyne cycloaddition to form FHMSNs-Pep1. The successful surface functionalization (FHMSNs-Pep1) was confirmed by Fourier transform infrared (FTIR) spectroscopy (Supplementary Figures S5 and S6). Doxorubicin (Dox) was selected as a model cargo, which was loaded into the pores of the

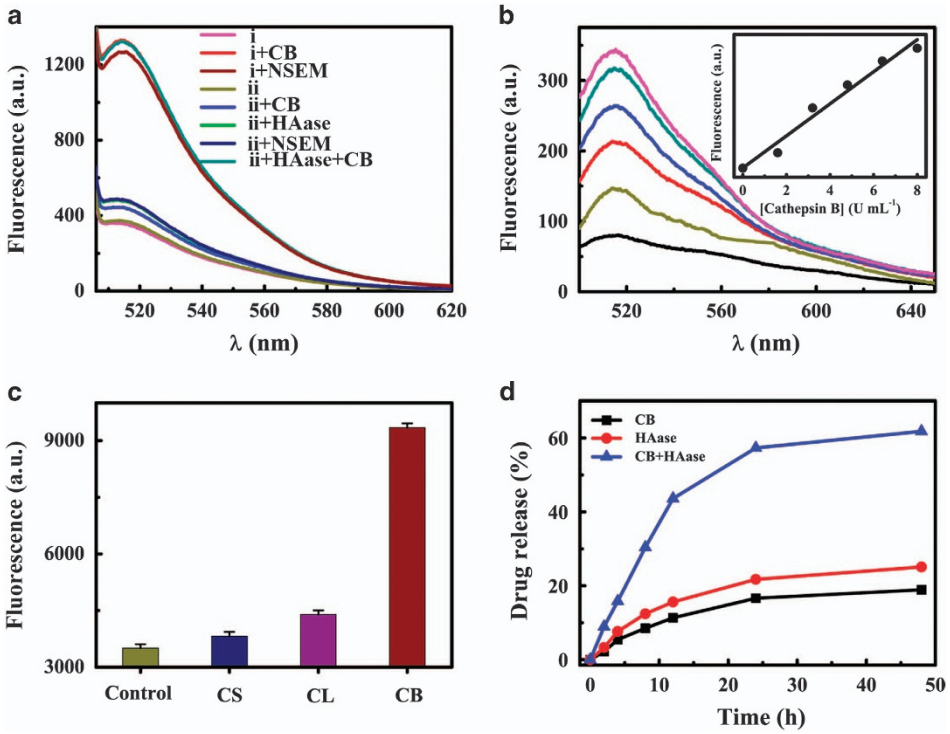

Figure 2 (**a**) Fluorescence emission spectra of unprotected nanovehicles ((i) FHMSNs@GNC) and self-protected nanovehicles ((ii) FHMSNs@GNC@HA) treated with different enzymatic species (Cat B (CB), a NSEM or HAase). (**b**) Fluorescence emission spectra of 0.1 mg ml^{-1} FHMSNs@GNC@HA upon addition of Cat B at increasing concentrations (0, 1.6, 3.2, 4.8, 6.4, 8 U ml^{-1}, respectively) after incubation with HAase. (**c**) Changes in the fluorescence spectra of the nanovehicles upon treatment with 5 U ml^{-1} of Cat B, Cat L, and Cat S, respectively; (**d**) The controlled drug release profiles of the nanovehicles with the addition of different enzymatic species in PBS (10 mM, pH = 5.0). Cat B, cathepsin B; Cat L, cathepsin L; Cat S, cathepsin S; FHMSNs, fluorescent, hollow mesoporous silica nanoparticles; GNCs, gold nanoclusters; HA, hyaluronic acid; HAase, hyaluronidase; NSEM, nonspecific enzymatic mixture; PBS, phosphate-buffered saline.

FHMSNs by mixing FHMSNs-Pep1 and Dox overnight (Dox-FHMSNs-Pep1). The amount of Dox loaded into the FHMSNs was determined to be 282 mg g^{-1} (Supplementary Figure S7). Then, the smart FHMSNs@GNC@HA nanovehicles were prepared by capping the pores with multifunctional gatekeepers consisting of orange-emitting GCNs[31] as a fluorescence quencher and HA as a protective shell via layer-by-layer assembly with two specific peptides: Pep1 for Cat B and Pep2 for HA. High-resolution transmission electron microscopy images provided direct evidence of the formation of the nanovehicles. Figure 1a, iv shows dark spots on the outside edges of the mesopores, representing the conjugation of the GNCs on the exterior surface of the FHMSNs. In addition, rough surfaces were present due to the different electron penetrability of the FHMSN cores and polymer (HA) shells, demonstrating the successful conjugation of HA.[32] The average diameter of the GNCs was 3.3 nm, which was optimal for capping the 3-nm-wide pores and preventing leakage of the entrapped Dox. The loading amount of the GNCs on the FHMSNs-P1 was optimized to 314 μg mg^{-1} by monitoring the fluorescence spectra of the GNCs in the supernatant and in the stock solutions. The HA content coated onto the surface of the nanoparticles was increased from 33 to 155 mg g^{-1} with the Pep2 conjugation, suggesting the successful assembly of Pep2 and its importance for the HA coating (Supplementary Figure S8). In addition, the gradual increase in the hydrodynamic diameter observed by dynamic light scattering and the reversed zeta potential further confirmed the successful assembly of the nanovehicles (Figure 1c).

In the core/satellite PMPs (FHMSNs@GNC), the fluorescence of the FHMSNs-Pep1 could be quenched by GNCs with a quenching efficiency of 92% (Figure 1b), suggesting an efficient energy transfer from the FHMSNs to the GNCs. Theoretical and experimental studies have shown that the distance-dependent quenching of gold nanoparticles with diameters of 1–20 nm follow a $1/r^4$ relationship, and this is termed NSET.[33] Unlike the Förster resonance energy transfer, whose efficiency is markedly dependent upon the spectral overlap level and separation distance (< 10 nm) between the donor fluorophore and the acceptor fluorophore, NSET maintains the quenching character even with a separation distance of 22 nm, ensuring that the majority of the dye doped in the mesoporous silica hollow shell (thickness ~ 20 nm) can be quenched. Thus, the hollow structure of the FHMSNs and the high sensitivity of NSET determines the high quenching efficiency,[34] creating a sensitive signal for probing proteases in living systems. By monitoring the variations in the fluorescence spectra of the nanovehicles with different HA densities treated with the nonspecific enzyme mixture (a mixture of trypsin (2 μg ml^{-1}), chymotrypsin (2 μg ml^{-1}) and MMP-2 (2 μg ml^{-1})), the amount of HA linked to the nanovehicles was optimized to be 0.08 mg mg^{-1} (Figure 1d), at which point the HA shell was thick enough to prevent the nonspecific enzymes from cleaving the substrate peptide and recovering the fluorescence.

Detection of Cat B and dual-enzyme controlled drug release *in vitro*

To test the self-protection function of the nanovehicles, the fluorescent properties of the nanovehicles were investigated under different conditions. As shown in Figure 2a, the unprotected core/satellite

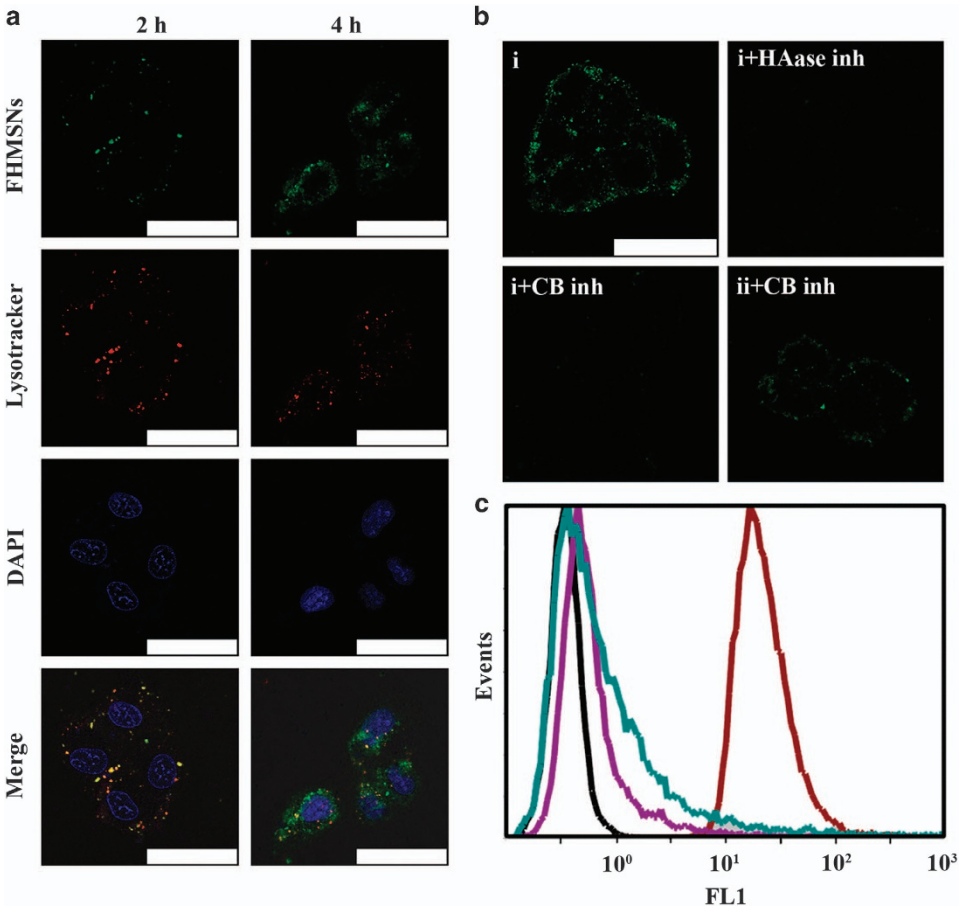

Figure 3 (**a**) CLSM images of HeLa cells incubated with the nanovehicles for 2 and 4 h. The green fluorescence from the FHMSNs shows the location of the nanovehicles. The red fluorescence from LysoTracker shows the location of acidic organelles such as lysosomes and endosomes, and the blue color shows cell nuclei stained with DAPI (The scale bar is 50 μm). (**b**) Cat B imaging in HeLa cells treated with HAase inhibitor (HAase inh) or Cat B inhibitor (CB inh) by the self-protected nanovehicles (i) and unprotected nanovehicles (ii) obtained using CLSM (The scale bar is 50 μm). (**c**) Fluorescence recovery of FHMSNs obtained by flow cytometry (Lines from left to right: control; incubation with HAase inhibitor; incubation with Cat B inhibitor; incubation without inhibitor). CLSM, confocal laser scanning microscopy; DAPI, 4,6-diamidino-2-phenylindole; FHMSNs, fluorescent, hollow mesoporous silica nanoparticles; HAase, hyaluronidase.

nanovehicles yielded high signals in the presence of the nonspecific enzymatic mixture (a mixture of trypsin (2 μg ml^{-1}), chymotrypsin (2 μg ml^{-1}) and MMP-2 (2 μg ml^{-1})), which is comparable to the signal intensity triggered by Cat B. For the self-protected core/satellite/shell nanovehicles, the addition of the enzymatic mixture left the fluorescent signal almost unaffected. Only when the HAase and Cat B existed simultaneously was the fluorescence of the nanovehicles recovered. Insight into the mechanism of protection from enzymolysis is provided by measurements in the presence or absence of HAase. The protective shell (HA shell) may impede access of the enzyme molecule to the core/satellite system. Once the protective shell was digested by HAase, the enzyme molecule was able to access Pep1 and the fluorescence recovery was triggered by the cleavage of the peptide.

Then, Cat B was detected by the nanovehicles in the presence of HAase. Figure 2b demonstrats that the fluorescence of the nanovehicles gradually recovered with the increase in Cat B concentrations. The inset in Figure 2b depicts the fluorescent signal as a function of Cat B concentration. Notably, the plot of the fluorescent signal against the concentrations of Cat B ranging from 0 to 8 U ml^{-1} displays a good linear relationship. This indicates that Cat B could specifically hydrolyze Pep1, thus dissociating GNCs from the surface of FHMSNs and invalidating the NSET process.

In addition, the selectivity of the nanovehicles for Cat B was investigated by detecting interference by other enzymes in the endosome. The changes in the fluorescence spectra of the nanovehicles originating from the FHMSNs treated with Cat B, cathepsin L (Cat L) and cathepsin S (Cat S) are described in Figure 2c. Compared to the analogues, only Cat B stimulated the effective fluorescence recovery of the nanovehicles, exhibiting high selectivity for Cat B among members of the cathepsin family, which could be attributable to the specific recognition and hydrolysis of Pep1.[35]

Furthermore, to investigate the dual-enzyme controlled drug release efficiency of the nanovehicles, drug release experiments were carried out in the presence and absence of HAase and Cat B, respectively. Real-time drug release profiles were recorded (Figure 2d). Only a negligible release of Dox was observed over a period of 48 h with the addition of HAase, indicating that the embedded core/satellite PMP remained intact. On the other hand, separate treatment with a high concentration of Cat B also revealed no significant release of Dox from the nanovehicles, which implied that the HA shell held the inner PMP via the specific interaction with Pep 2 and hindered enzymatic digestion. While in the presence of both HAase and Cat B, burst and continuous Dox release was observed as time progressed. In addition, the dosage of the released Dox was dependent on Cat B

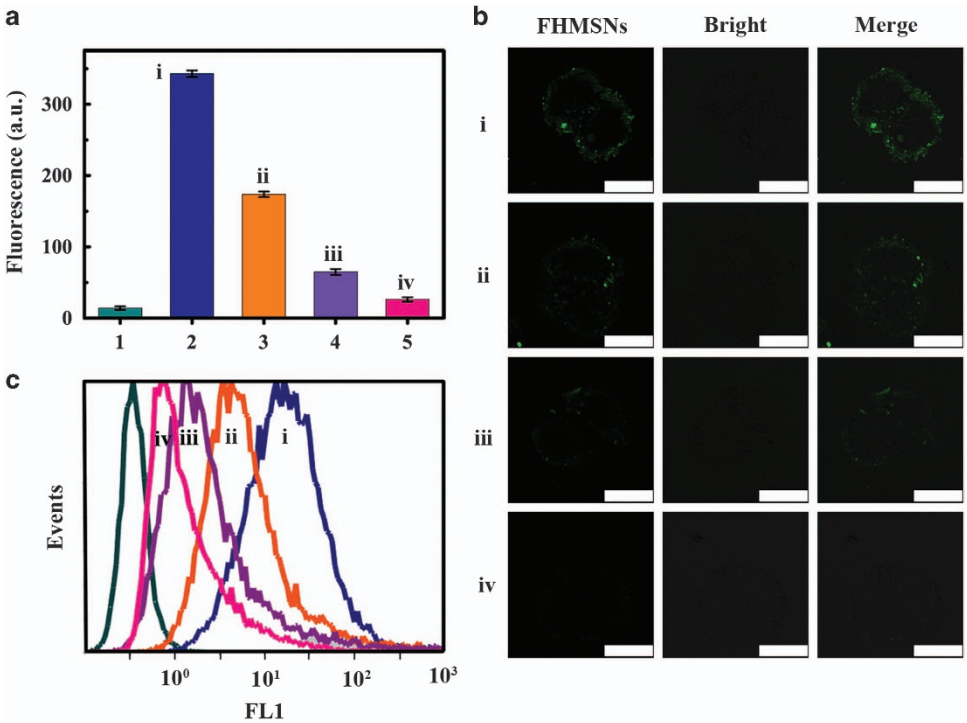

Figure 4 (**a**) Cat B activity in HeLa cells after different treatments detected using a Cat B activity assay kit (1: control, 2: cell lysate, 3: cell lysate+100 μmol Cat B inhibitor, 4: cell lysate+200 μmol Cat B inhibitor, 5: cell lysate+400 μmol Cat B inhibitor). (**b**) Cat B imaging of HeLa cells by the nanovehicles obtained using CLSM (The scale bar is 25 μm). The cells treated with different concentrations of Cat B inhibitor ((i) no inhibitor, (ii) 1 μmol, (iii) 2 μmol, (iv) 4 μmol) were incubated with the nanovehicles at 37 °C for 4 h. (**c**) Fluorescence recovery of FHMSNs obtained by flow cytometry ((i) no inhibitor, (ii) 10 μmol, (iii) 20 μmol, (iv) 40 μmol). Cat B, cathepsin B; CLSM, confocal laser scanning microscopy; FHMSNs, fluorescent, hollow mesoporous silica nanoparticles.

concentrations, wherein a concentration of 8 U ml^{-1} lead to fast and efficient release (Supplementary Figure S9). This suggested that the disassembly of the nanovehicles accompanied by the efficient release of Dox was synergistically triggered by a combination of HAase and Cat B inside the cells.

Specific targeting uptake and subcellular distribution

Targeted delivery to cancer cells is necessary for accurate intracellular imaging of proteases. Herein, HA, which specifically recognizes CD44 and RHAMM receptors overexpressed on the surface of some cancer cells,[27,28] was tethered to the nanovehicles, acting not only as a protecting shell but also as a target ligand. To verify the HA-mediated active targeting of the nanovehicles, HeLa cells (positive control) and NIH-3T3 cells (negative control) were incubated with different formulations containing Dox. The target efficiency and specificity of the nanovehicles were assessed by CLSM and flow cytometry analysis by determining the fluorescence of the recovered FHMSNs and the loaded Dox (Supplementary Figure S10). Both the emitted fluorescence of the recovered FHMSNs and the loaded Dox from HeLa cells were higher than those from NIH-3T3 cells, which reflected enhanced uptake due to the specific interaction between HA and the receptors. Compared with Dox-FHMSNs-Pep1 without the HA shell, the flow cytometric results shown in Supplementary Figure S10 further confirmed that Dox-FHMSNs@GNC@HA showed significantly enhanced uptake in HeLa cells but decreased uptake in NIH-3T3 cells, indicating that receptor-mediated endocytosis plays an important role in facilitating the intracellular accumulation of the nanovehicles.

Furthermore, CLSM was used to investigate the traceability of the nanovehicles during intracellular delivery. HeLa cells were incubated in cultured medium containing 20 μg ml^{-1} of the nanovehicles at 37 °C for a period of time. The intracellular trafficking of the nanovehicles was investigated by monitoring the recovered fluorescence of FHMSNs. After 2 h of incubation, the signal of the nanovehicles (green) was mainly colocalized with the signal of LysoTracker (red), a late endosome and lysosome marker, indicating that the nanovehicles were effectively taken up by the cells and entrapped into the endosomes (Figure 3a). After an additional 2 h of incubation, a large dissociation in the signals between nanovehicles and LysoTracker was observed, confirming the efficient endosomal escape of the nanovehicles. By co-staining with DAPI molecules, it was found that the nanovehicles were mostly distributed in the cytoplasm. It is worth noting that the fluorescence signal of FHMSNs was enhanced when the incubation time was extended, which could be due to the progress of the disassembly of the nanovehicles in response to intracellular Cat B, indicating that the nanovehicles have the potential for use in intracellular imaging of Cat B.

Intracellular imaging of Cat B

We further investigated whether the nanovehicles could be used for intracellular imaging of Cat B by detecting the fluorescence recovery of FHMSNs. First, the validity of the self-protection of nanovehicles was verified by estimating the role of HAase and Cat B in the disassembly of nanovehicles in cells by monitoring the fluorescence recovery via CLSM and flow cytometry. After incubation with the self-protected nanovehicles at 37 °C for 6 h, significant fluorescence recovery was observed, which suggested the disassembly of the nanovehicles inside

the cells (Figure 3b). In sharp contrast, HeLa cells pretreated with HAase inhibitor (TG, 4 μM) exhibited much a dimmer fluorescence than did the untreated cells, which indicated that the nanovehicles maintained structural integrity inside the cells because of the blocking of HAase-mediated HA degradation. As expected, the Cat B inhibitor (antipain hydrochloride, 4 μM)-treated cells presented no remarkable recovery in fluorescence, suggesting that the inner PMPs remained intact even though the HA shell had been degraded by HAase, owing to the failure of the Cat B-mediated Pep1 degradation. While incubated with the unprotected nanovehicles, the Cat B-inhibited cells still showed bright fluorescence, indicating that the unprotected PMPs were unstable and easily generated a false signal. Furthermore, the flow cytometry experiments also revealed that the recovered fluorescence intensity was significantly reduced in the presence of either the HAase inhibitor or the Cat B inhibitor (Figure 3c). These experiments clearly suggest that the dissociation of the nanovehicles was specifically induced by the two enzymes HAase and Cat B in a synergistic manner.

Next, the expression levels of Cat B were evaluated with the nanovehicles by using CLSM and flow cytometry. Intracellular Cat B content was regulated by treating cells with different concentrations of Cat B inhibitor prior to incubation with the nanovehicles at 37 °C for 6 h. The downregulation of Cat B content resulting from Cat B inhibitor-induced cells was verified using a commercial Cat B activity assay kit (Figure 4a). With the downregulation of intracellular Cat B content, the fluorescence intensity was observed to decrease in both the CLSM (Figure 4b) and flow cytometric (Figure 4c) results, which was in agreement with the results obtained from the Cat B activity assay kit. These results suggested that the nanovehicles can be specifically activated in Cat B-expressing cells, thereby providing a nanosensor for the *in situ* visualization and evaluation of endogenous Cat B activity in living cells.

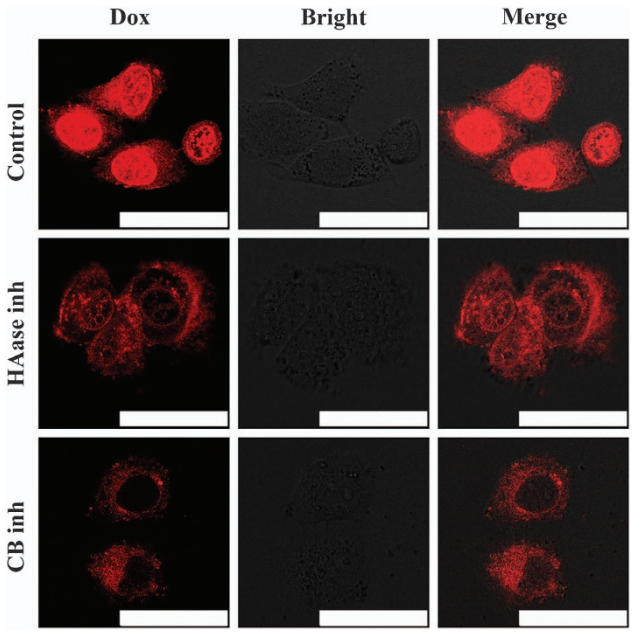

Figure 5 CLSM images of HeLa cells treated with HAase inhibitor (HAase inh) or Cat B inhibitor (CB inh) after incubation with the nanovehicles for 24 h (The scale bar is 50 μm). Cat B, cathepsin B; CLSM, confocal laser scanning microscopy; HAase, hyaluronidase.

Controlled drug release within the cells and selective toxicity

To demonstrate the intracellular dual-enzyme controlled Dox release from the nanovehicles, we inhibited HAase or Cat B production in the cells by adding inhibitors prior to the addition of the nanovehicles. The fluctuation in intracellular HAase or Cat B concentration can result in a change in the extent of GNCs dissociated from the nanovehicles, which was consistent with the amount of released Dox. As shown in Figure 5, treatment with either the HAase inhibitor or the Cat B inhibitor had a remarkable impact on the release of Dox. Clearly, the nanovehicles impeded drug leakage under circumstances of inadequate HAase or Cat B but collapsed to efficiently release the encapsulated drug in response to combined HAase and Cat B stimuli, both of which were highly expressed inside the tumor cells. To further evaluate the intracellular dual-enzyme controlled release of the drugs

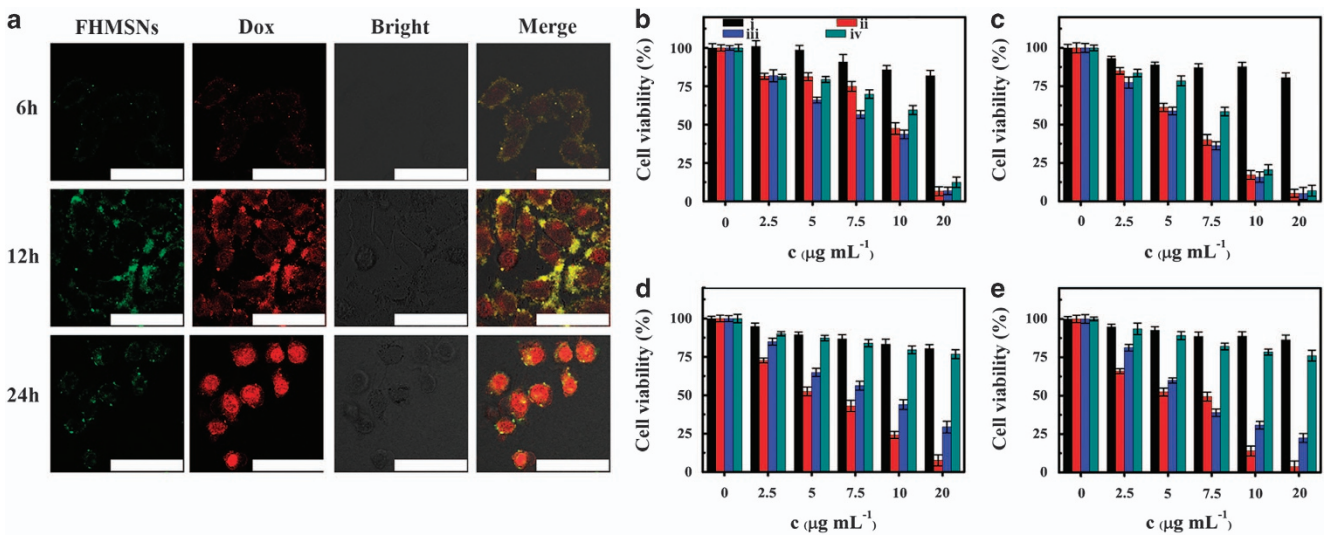

Figure 6 (**a**) CLSM images of HeLa cells incubated with Dox-FHMSNs@GNC@HA for different times (The scale bar is 75 μm). Cell viability of HeLa cells (**b**: 24 h, **c**: 48 h) and NIH-3T3 cells (**d**: 24 h, **e**: 48 h) incubated with different concentrations of FHMSNs@GNC@HA (i), Dox-FHMSNs-Pep1 (ii) Dox-FHMSNs@GNC (iii) and Dox-FHMSNs@GNC@HA (iv) for 24 and 48 h, respectively. CLSM, confocal laser scanning microscopy; FHMSNs, fluorescent, hollow mesoporous silica nanoparticles; GNCs, gold nanoclusters; HA, hyaluronic acid; Pep1, peptide 1.

accompanied by the disassembly of Dox-containing nanovehicles, the fluorescence change was monitored using CLSM after the cells had been incubated with the nanovehicles containing Dox over time (Figure 6a). After 6 h of incubation, the signal of recovered FHMSNs (green) that was used to label the nanovehicles was mostly overlaid with the signal of Dox (red), implying that Dox was embedded in the nanovehicles. Note that the increased FHMSNs and Dox signals showed obvious separation after incubation for an additional 6 h, suggesting efficient intracellular release and cytoplasmic distribution of Dox due to the detachment of HA and GNCs in response to intracellular HAase and Cat B. After additional 12 h, most of the cells had undergone apoptosis, along with the appearance of massive apoptotic bodies, suggesting a high therapeutic efficacy of the nanovehicles. The decreased fluorescence intensity of FMSNs after 24 h incubation may be due to the apoptosis-induced increase in cell membrane permeability and the accelerated nanoparticle diffusion.[36]

Furthermore, MTT tests were conducted to elucidate the therapeutic potential of the nanovehicles. A cancer cell growth inhibitor effect was observed in HeLa cells and NIH-3T3 cells after treatment with FHMSNs@GNC@HA, Dox-FHMSNs-Pep1, Dox-FHMSNs@GNC or Dox-FHMSNs@GNC@HA. As shown in Figures 6b–e, blank nanovehicles without Dox did not show cytotoxicity within the tested concentration range. The toxicity of Dox-FHMSNs-Pep1 was approximately equal for NIH-3T3 cells and HeLa cells. After capping by GNCs, the nanovehicles exhibited much higher toxicity to HeLa cells than to NIH-3T3 cells due to the overexpression of Cat B within HeLa cells. Moreover, the nanovehicles exhibited much higher toxicity after further encapsulation by HA owing to the specific recognition of HA. Then, HeLa cells were incubated with different concentrations of Dox in different formulations at 37 °C for 24 or 48 h. As shown in Supplementary Figure S11, the lethality of free Dox at the microgram level was very small due to the effect of ATP-binding cassette transporters acting as drug efflux pumps from the cytoplasm.[37] On the other hand, given the specific targeting by HA and the dual-enzyme controlled drug release, the cellular uptake of Dox-FHMSNs@GNC@HA was higher than that of Dox-FHMSNs@GNC, which led to better anticancer activity.

CONCLUSIONS

In conclusion, we fabricated self-protected nanovehicles for the precise imaging of intracellular Cat B and dual enzyme-controlled drug release based on a peptide-mediated core/satellite/shell assembly. Using this core/satellite PMP system, Cat B activity was detected with high sensitivity from the FHMSN fluorescence recovery caused by the specific cleavage of the bridge peptide between the signal donor and acceptor. The HA shell was the protective layer and target ligand and guaranteed that the internal PMP structure had not been degraded and that the probe was efficiently taken up, leading to higher sensitivity and selectivity for protease detection than with conventional unprotected nanoprobes. Making use of Cat B-induced detachment of GNCs, a gated drug release system in response to the Cat B activity was constructed, which exhibited high efficacy for tumor cell inhibition and good applicability for drug release monitoring. Integrating the functions of *in situ* probing of intracellular proteases, targeted drug delivery and pinpoint release, and real-time evaluation of drug release processes into one entity, this nanovehicle provides a promising platform for the exploration of precise cancer diagnostic and therapeutic strategies.

CONFLICT OF INTEREST

The authors declare no conflict of interest.

ACKNOWLEDGEMENTS

We gratefully appreciate the support from the National Natural Science Foundation of China (Nos: 21335004, 21575061, 21622505). F.Z. is also grateful for support from Program B for Outstanding Ph.D. Candidate of Nanjing University.

1 Lopez-Otin, C. & Overall, C. M. Protease degradomics: a new challenge for proteomics. *Nat. Rev. Mol. Cell Biol.* **3**, 509–519 (2002).
2 Krane, S. M. Elucidation of the potential roles of matrix metalloproteinases in skeletal biology. *Arthritis Res. Ther.* **5**, 2–4 (2003).
3 Yang, Y., Hill, J. W. & Rosenberg, G. A. Multiple roles of metalloproteinases in neurological disorders. *Prog. Mol. Biol. Transl. Sci.* **99**, 241–263 (2011).
4 van Kempen, L. C., de Visser, K. E. & Coussens, L. M. Inflammation, proteases and cancer. *Eur. J. Cancer* **42**, 728–734 (2006).
5 Luttun, A., Dewerchin, M., Collen, D. & Carmeliet, P. The role of proteinases in angiogenesis, heart development, restenosis, atherosclerosis myocardial ischemia, and stroke: insights from genetic studies.. *Curr. Atheroscler. Rep.* **2**, 407–416 (2000).
6 Aggarwal, N. & Sloane, B. F. Cathepsin B: multiple roles in cancer. *Proteomics Clin. Appl.* **8**, 427–437 (2014).
7 Lowe, S. B., Dick, J. A. G., Cohen, B. E. & Stevens, M. M. Multiplex sensing of protease and kinase enzyme activity via orthogonal coupling of quantum dot peptide conjugates. *ACS Nano* **6**, 851–857 (2012).
8 Ghadiali, J. E., Lowe, S. B. & Stevens, M. M. Quantum-dot based FRET detection of histone acetyltransferase activity. *Angew. Chem. Int. Ed.* **50**, 3417–3420 (2011).
9 Olson, E. S., Jiang, T., Aguilera, T. A., Nguyen, Q. T., Ellies, L. G., Scadeng, M. & Tsien, R. Y. Activatable cell penetrating peptides linked to nanoparticles as dual probes for *in vivo* fluorescence and MR imaging of proteases. *Proc. Natl Acad. Sci. USA* **107**, 4311–4316 (2010).
10 Thurley, S., Roglin, L. & Seitz, O. Hairpin peptide beacon: dual-labeled PNA-peptide-hybrids for protein detection. *J. Am. Chem. Soc.* **129**, 12693–12695 (2007).
11 Mura, S., Nicolas, J. & Couvreur, P. Stimuli-responsive nanocarriers for drug delivery. *Nat. Mat.* **12**, 991–1003 (2013).
12 Kelley, E. G., Albert, J. N. L., Sullivan, M. O. & Epps, T. H. Stimuli-responsive copolymer solution and surface assemblies for biomedical applications. *Chem. Soc. Rev.* **42**, 7057–7071 (2013).
13 Blum, A. P., Kammeyer, J. K., Rush, A. M., Callmann, C. E., Hahn, M. E. & Gianneschi, N. C. Stimuli-responsive nanomaterials for biomedical applications. *J. Am. Chem. Soc.* **137**, 2140–2154 (2015).
14 Lu, Y., Aimetti, A. A., Langer, R. & Gu, Z. Bioresponsive materials. *Nat. Rev. Mater.* **1**, 16075 (2016).
15 Du, J. Z., Du, X. J., Mao, C. Q., Wang, J. & Tailor-Made Dual, pH-Sensitive Polymer–doxorubicin nanoparticles for effient anticancer drug delivery. *J. Am. Chem. Soc.* **133**, 17560–17563 (2011).
16 Zhang, P. H., Wang, C., Zhao, J. J., Xiao, A. Q., Shen, Q., Li, L. T., Li, J. X., Zhang, J. F., Min, Q. H., Chen, J. N., Chen, H. Y. & Zhu, J. J. Near infrared-guided smart nanocarriers for microRNA-controlled release of doxorubicin/siRNA with intracellular ATP as fuel. *ACS Nano* **10**, 3637–3647 (2016).
17 Bernardos, A., Mondragón, L., Aznar, E., Marcos, M. D., Martínez-Máñez, R., Sancenón, F., Soto, J., Barat, J. M., Pérez-Payá, E., Guillem, C. & Amorós, P. Enzyme-responsive intracellular controlled release using nanometric silica mesoporous supports capped with 'Saccharides'. *ACS Nano* **4**, 6353–6368 (2010).
18 Ong, W., Yang, Y., Cruciano, A. C. & McCarley, R. L. Redox-triggered contents release from liposomes. *J. Am. Chem. Soc.* **130**, 14739–14744 (2008).
19 Chen, K. J., Liang, H. F., Chen, H. L., Wang, Y., Cheng, P. Y., Liu, H. L., Xia, Y. & Sung, H. W. A thermoresponsive bubble-generating liposomal system for triggering localized extracellular drug delivery. *ACS Nano* **7**, 438–446 (2013).
20 Ruiz-Hernández, E., Baeza, A. & Vallet-Regí, M. Smart drug delivery through DNA/magnetic nanoparticle gates. *ACS Nano* **5**, 1259–1266 (2011).
21 Rapoport, N. Y., Kennedy, A. M., Shea, J. E., Scaife, C. L. & Nam, K. H. Controlled and targeted tumor chemotherapy by ultrasound-activated nanoemulsions/microbubbles. *J. Control. Release* **138**, 268–276 (2009).
22 Xiao, Z. Y., Ji, C. W., Shi, J. J., Pridgen, E. M., Frieder, J., Wu, J. & Farokhzad, O. C. DNA self-assembly of targeted near-infrared-responsive gold nanoparticles for cancer thermo-chemotherapy. *Angew. Chem. Int. Ed.* **54**, 11853–11857 (2012).
23 Ge, J., Neofytou, E., Cahill, T. J., Beygui, R. E. & Zare, R. N. Drug release from electric-fild-responsive nanoparticles. *ACS Nano* **6**, 227–233 (2011).
24 Ghadiali, J. E. & Stevens, M. M. Enzyme-responsive nanoparticle systems. *Adv. Mater.* **20**, 4359–4363 (2008).
25 Mohamed, M. M. & Sloane, B. F. Cysteine cathepsins: multifunctional enzymes in cancer. *Nat. Rev. Cancer* **6**, 764–775 (2006).
26 Singh, A., Corvelli, M., Unterman, S. A., Wepasnick, K. A., McDonnell, P. & Elissee, J. H. Enhanced lubrication on tissue and biomaterial surfaces through peptide-mediated binding of hyaluronic acid. *Nat. Mat.* **13**, 988–995 (2014).
27 Gotte, M. & Yip, G. W. Heparanase, hyaluronan, and CD44 in cancers: a breast carcinoma perspective. *Cancer Res.* **66**, 10233–10237 (2006).

28 Qhattal, H. S. S. & Liu, X. Characterization of CD44-mediated cancer cell uptake and intracellular distribution of hyaluronan-grafted liposomes. *Mol. Pharmaceutics* **8**, 1233–1246 (2011).
29 Stern, R. & Jedrzejas, M. J. Hyaluronidases: their genomics, structures, and mechanisms of action. *Chem. Rev.* **106**, 818–839 (2006).
30 Chen, F., Hong, H., Shi, S., Goel, S., Valdovinos, H. F., Hernandez, R., Theuer, C. P., Barnhart, T. E. & Cai, W. Engineering of hollow mesoporous silica nanoparticles for remarkably enhanced tumor active targeting efficacy. *Sci. Rep.* **4**, 1–10 (2014).
31 Luo, Z., Yuan, X., Yu, Y., Zhang, Q., Leong, D. T., Lee, J. Y. & Xie, J. From aggregation-induced emission of Au(I)–thiolate complexes to ultrabright Au(0)@Au(I)–thiolate core–shell nanoclusters. *J. Am. Chem. Soc.* **134**, 16662–16670 (2012).
32 Zhang, X., Yang, P., Dai, Y., Ma, P., Li, X., Cheng, Z., Hou, Z., Kang, X., Li, C. & Lin, J. Multifunctional up-converting nanocomposites with smart polymer brushes gated mesopores for cell imaging and themo/pH dual-responsive drug controlled release. *Adv. Funct. Mater.* **23**, 4067–4078 (2013).
33 Yun, C. S., Javier, A., Jennings, T., Fisher, M., Hira, S., Peterson, S., Hopkins, B., Reich, N. O. & Strouse, G. F. Nanometal surface energy transfer in optical rulers, breaking the FRET barrier. *J. Am. Chem. Soc.* **127**, 3115–3119 (2005).
34 Zheng, F. F., Zhang, P. H., Xi, Y., Chen, J. J., Li, L. L. & Zhu, J. J. Aptamer/graphene quantum dots nanocomposite capped fluorescent mesoporous silica nanoparticles for intracellular drug delivery and real-time monitoring of drug release. *Anal. Chem.* **87**, 11739–11745 (2015).
35 Chowdhury, M. A., Moya, I. A., Bhilocha, S., McMillan, C. C., Vigliarolo, B. G., Zehbe, I. & Phenix, C. P. Prodrug-inspired probes selective to cathepsin B over other cysteine cathepsins. *J. Med. Chem.* **57**, 6092–6104 (2014).
36 Hessler, J. A., Budor, A., Putchakayala, K., Mecke, A., Rieger, D., Holl, M. M. B. & Orr, B. G. Atomic force microscopy study of early morphological changes during apoptosis. *Langmuir* **21**, 9280–9286 (2005).
37 He, Q. J. & Shi, J. L. MSN anti-cancer nanomedicines: chemotherapy enhancement, overcoming of drug resistance, and metastasis inhibition. *Adv. Mater.* **26**, 391–411 (2014).

Supplementary Information accompanies the paper on the NPG Asia Materials website (http://www.nature.com/am)